Tamara Harms, University of Alaska Fairbanks
Waterbody Field Report[1, 2]
Salcha River, Salcha, Alaska

Prepared by: T. Harms

Abstract

Water quality was monitored in the Salcha River 5/18/2021-9/30//2021 and 5/3/2022-10/8/2022 to determine whether the river is influenced by non-point source pollution. A sonde collected measurements of turbidity, fluorescent dissolved organic matter, specific conductivity, pH, dissolved oxygen, and temperature every 15 minutes. Grab samples were collected approximately biweekly for analysis of nitrogen, phosphorus, dissolved organic carbon, and major anions and cations in the laboratory. Water chemistry of the Salcha River was similar to other upland streams and rivers of Interior Alaska, characterized by relatively high concentrations of base cations (calcium, magnesium), sulfate, and nitrate, and low concentrations of ammonium and phosphorus. Measured chemical constituents did not exceed Alaska water quality standards, though summertime water temperature exceeded thresholds established for anadromous salmonids.

Water chemistry data were analyzed to characterize sources of solutes to the mainstem Salcha River and to estimate metabolism (gross primary production and ecosystem respiration) in the river. A mixing model indicated that solutes were derived largely from snowmelt during the spring freshet, with increasing contributions from tributaries draining south-facing catchments as flow receded. Turbidity and fDOM concentrations increased on the rising limb of most storms, indicating rapid flushing of these materials via surficial flowpaths from the catchment to the stream. In contrast, specific conductivity was typically diluted during storms, likely due to dilution of mineral-rich groundwater by shallower flowpaths. Instream gross primary production was low (maximum ~2.5 mg C $m^{-2}d^{-1}$), but sustained throughout the open-water period following snowmelt recession, with a peak during warm conditions in late June, and decreases following storms.

Table 1. Waterbody description.

Assessment Unit ID	AK_R_8030508_008
Assessment Unit Name	Salcha River
Location description	Salcha River, at USGS gauging house upstream of Richardson Highway bridge
Hydrologic unit code	19040505
Water Type	river
Area sampled	water column
Time of year sampled	Snowmelt-autumn

Water Quality Evaluation

Background

The Salcha River was monitored to determine whether water quality is influenced by non-point source pollution (Table 1). The watershed is located in the boreal biome of Interior Alaska and the Salcha is a major tributary (contributing area 5740 km^2) of the Tanana River (Fig. 1). The river drains largely undeveloped lands and is used for recreation. A water chemistry monitoring program was carried out

[1] Nonpoint Source Pollution, Water Quality, Division of Water, Department of Environmental Conservation

[2] This project has been funded wholly or in part by the United States EPA under assistance agreement number 00J84604 to the Department of Environmental Conservation through the Alaska Clean Water Actions (ACWA) program. The contents of this document do not necessarily reflect the views and policies of the EPA, nor does the EPA endorse trade names or recommend the use of commercial product mentioned in this document.

during the open-water periods of 2021 & 2022, at a site on the mainstem adjacent to the USGS discharge gauging station (#15484000), ~3 km upstream of the confluence with the Tanana River.

Interior Alaska has a continental climate with cold winters, and warm, relatively dry summers. Mean annual air temperature (1992-2022) for Interior Alaska near Fairbanks is –3.4 °C with the lowest mean monthly temperature typically in January (–23.0°C) and the highest mean monthly temperature in July (15.1°C), as measured by the Bonanza Creek Long-Term Ecological Research Program (http://bnznet.iab.uaf.edu/vdv/index.html). During the study period (2021-2022), temperatures were similar to the long-term average, with exceptions of May and September temperatures ~ 1°C colder than average in 2022 and 2021 respectively, and September ~1°C warmer than average in 2022. Mean annual

Figure 1. Sampling location on the Salcha River located SE of Fairbanks, AK.

precipitation is 304 mm with 238 mm falling between June and August. Summer precipitation was greater than average in 2021 (307 mm) and lower than average in 2022 (146 mm).

Objective
Determine whether water quality of the Salcha River is influenced by non-point source pollution

Quality Assurance Review
The QAPP was followed for field data collection and for laboratory analyses with the following exceptions. Concentrations of dissolved organic carbon (DOC) were measured following the QAPP and were re-analyzed for verification from frozen samples stored for 1-12 months. The QAPP is attached to this report as an appendix.

Methods
Data collection and handling

Measurements of water chemistry were made at 15-min frequency using an EXO multi-parameter sonde (YSI, Inc.) equipped with optical sensors measuring dissolved oxygen (DO), turbidity, and fluorescent dissolved organic (fDOM) matter; and additional sensors measuring pH, temperature, and conductivity. An instream sonde was deployed to collect high-frequency measurements because water chemistry of this region typically changes rapidly during storms. Probes were calibrated in certified standards (pH, turbidity, conductivity), an internally verified standard (fDOM), or in moist air (DO) prior to deployment. Probes were checked for drift and fouling in deionized water or in pH buffer approximately biweekly. The pH and DO probes were recalibrated when these checks differed by more than 0.3 pH units or 5% from expected DO concentration. The sonde was deployed approximately 10-cm above the streambed. A burst of 9-12 observations was made by each sensor during a 30-s interval at each 15-min measurement interval. Resulting data were cleaned with automated routines to remove out-of-water points and uncertain measurements indicated by standard deviation (SD) of burst measurements greater than 5 times the mean SD of all bursts for each parameter in each year's record. Baseline drift was corrected manually based on readings in water or pH buffer and outliers were manually removed.

Grab samples were collected near the EXO sonde approximately every two weeks and handled according to the QAPP (Appendix 2). On 29 July 2021, five tributaries were sampled, as well as collection from the mainstem downstream of each tributary junction (Fig. 2). Grab samples were analyzed for concentrations of major anions by ion chromatography (ICS-2100, Thermo Scientific). Dissolved organic carbon and total dissolved nitrogen (TDN) were measured by combustion followed by non-dispersive infrared gas analysis and chemiluminescence, respectively (Shimadzu TOC/TN-L). Total dissolved phosphorus (TDP) was analyzed colorimetrically on a discrete autoanalyzer using the molybdate blue method following acid-persulfate digestion (Smartchem 170). Concentrations less than the lowest calibration standard for each analyte were replaced with the midpoint of zero and the limit of quantitation.

Storm concentration-discharge analysis

We analyzed concentration (C)-discharge (Q) relationships during storms from the high-freqency (15-min) observations collected by the EXO sonde and discharge reported by the adjacent USGS gauge. Storms were delineated manually and defined by cumulative precipitation greater than 5 mm in the preceding 24-hour period accompanied by both an increase in discharge and a change in stream chemistry. The start of each storm was the inflection point when discharge began to rise and the end was defined by return of discharge the pre-event flow or when another storm began.

We used summary metrics to compare storm-scale C-Q dynamics across events and constituents. The Hysteresis Index (HI) describes hysteresis in the C-Q relationship and was calculated as:

$$HI = C_{RL} - C_{FL}$$

where C_{RL} and C_{FL} are event-normalized concentrations on the rising and falling limb, respectively, calculated at 2% intervals of discharge (Lloyd et al., 2016). Subsequent analyses are based on the median and bootstrapped 95% CI of this distribution for each storm (Webster et al., 2021). HI is scaled between – 1 and 1 with negative values indicating counterclockwise hysteresis (greater concentration relative to discharge on the falling compared to rising limb of the storm) and positive values indicating clockwise hysteresis (greater concentration relative to discharge on the rising compared to falling limb of the storm). Counterclockwise hysteresis results when the constituent is delivered from storage pools in the catchment located distal to the stream, or limitation of constituent delivery by hydrologic transport. Clockwise hysteresis results from nearstream sources of the constituent to the stream, or limited pool size of the constituent relative to hydrologic transport. We additionally calculated a metric summarizing flushing and dilution dynamics during storms as the slope of the log C-Q relationship on the rising limb of each storm (β) with corresponding 95% confidence interval (Godsey et al., 2009). Positive β indicates flushing (concentration increase), negative β indicates dilution, and values of β with 95% CIs encompassing 0 indicate chemostatic behavior.

We used multiple regression models to evaluate the influence of storm size and intensity, antecedent moisture conditions, and seasonality on C-Q dynamics during storms. Storm intensity was estimated as the total precipitation during a storm event divided by event duration (mm/hr) and size was total precipitation during the event. We also summarized cumulative precipitation in intervals of one week, one month, and three months prior to each storm. Seasonality was summarized as time since peak flow during snowmelt, which standardized for differences in the timing of snowmelt between the two years. We eliminated predictor variables that were correlated (variance inflation factors > 2). Predictor variables were centered and standardized such that reported regression coefficients represent the change in storm C-Q response resulting from a 1 SD change in the predictor variable. Variance explained by fixed effects was quantified by R^2 values.

Sources of water and solutes to the mainstem

We estimated the proportion of water contributed to the Salcha River from precipitation and five major tributaries during the summers of 2021 and 2022. End members included water collected from Butte, Flat, McCoy, Ninetyeight and Redmond creeks above their confluence with the Salcha River (Fig.2, Table 2) and precipitation collected in the Goldstream Valley of Interior Alaska during the summer of 2021. We selected chloride, sulfate, magnesium, and sodium as tracers because they sufficiently bounded the mainstem water samples. Chloride and sodium are widely used as conservative tracers, and sulfate and magnesium can act as conservative in some environments or when present at sufficiently high concentrations (De Filippi et al. 2021, Schemel et al. 2006, Bencala et al. 1987).

Table 2. Attributes of sampled catchments. Contributing areas are depicted in Fig. 2.

Site	latitude	longitude	Area (km^2)
Butte	64.64289	-145.8812	138.2
Flat	64.58539	-146.1279	283.0
McCoy	64.51451	-146.3976	286.0
Ninetyeight	64.54965	-146.2642	64.8
Redmond	64.48852	-146.5619	220.8
Salcha mainstem	64.47143	-146.9281	5739.2

We used a Bayesian mixing model to estimate the contribution of these potential sources of solutes to the mainstem Salcha monitored near the USGS gauging station. Water samples from each sampling day on the mainstem were included as mixtures, and the sampling date was included as a random effect to produce an estimate for each date. We included both process and residual error in the model. The model was run for 100,000 iterations, and model convergence was assessed using the Gelman, Heidelberger and Welch, and Geweke diagnostics. The mixing model was implemented using the *MixSIAR* package for R (Stock et al. 2018).

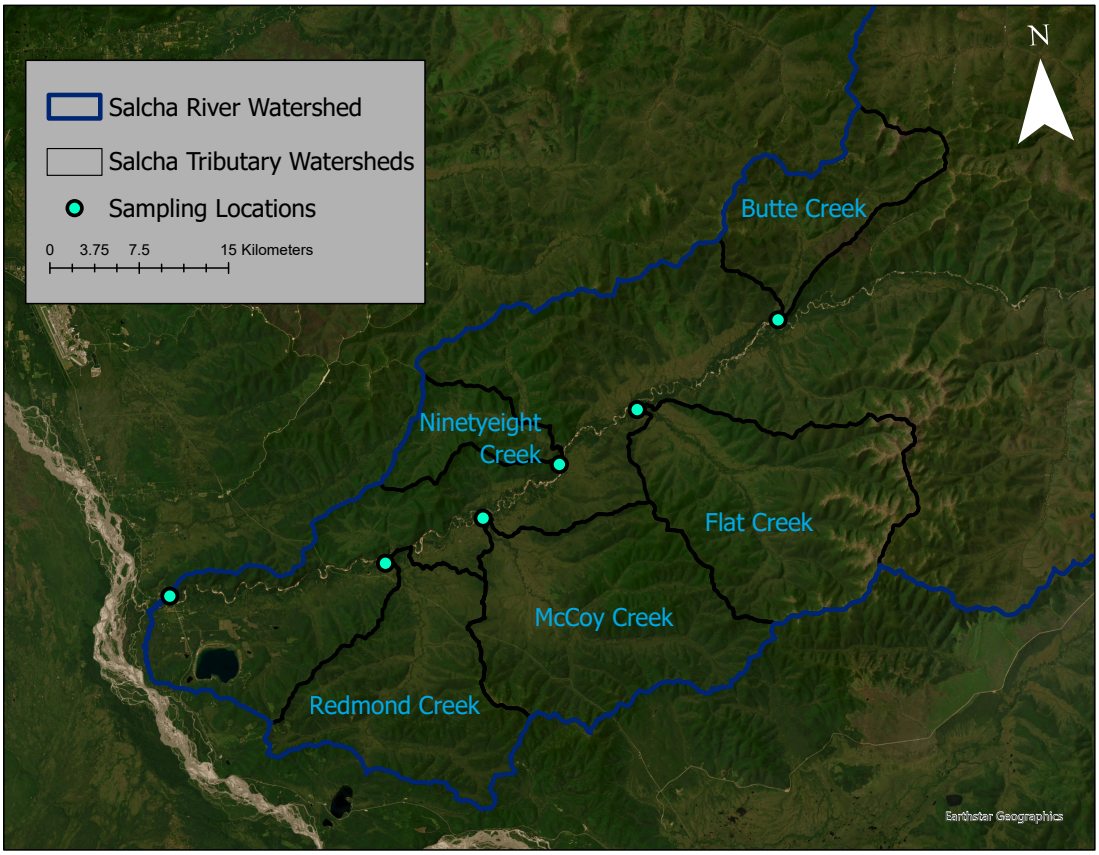

Fig. 2. Locations of tributary sampling in July 2022 relative to the location of sensor deployment and periodic grab sampling on the mainstem.

Whole-stream metabolism

Estimates of gross primary productivity (GPP), ecosystem respiration (ER), and gas evasion (K) were modeled from diurnal patterns in dissolved oxygen, light, and water temperature. This model is based on the DO budget summarized by Eq. 1 (Odum 1956):

$$(1)\ \frac{dO_t}{dt} = P_t + R_t + K_t$$

where the rate of change in dissolved oxygen concentration is determined by the rate of productivity (P_t) at time t, rate of oxygen removal by respiration (R_t), and the rate of air-water oxygen exchange (D_t). We applied a Bayesian inverse model to determine rates of these processes, implemented in the R package *StreamMetabolizer* (Appling et al. 2018). The inverse model uses multi-day time series of measured DO concentration, water temperature, river discharge, and light incident to the stream surface. Light was modeled from latitude, longitude, and date. The inverse model fits the parameters gross primary productivity (GPP; g O_2 m^{-2} d^{-1}), ecosystem respiration (ER, autotrophic plus heterotrophic respiration; g O_2 m^{-2} d^{-1}), and gas exchange rate (K_2; g O_2 m^{-2} d^{-1}) in Eqns 2-4. The areal rate of productivity, P_t is estimated by Eq. 2:

$$(2)\ P_t = \frac{GPP}{z} \times \frac{(t_1 - t_0)\, PPFD_t}{\int_{u=t_0}^{t_1} PPFD_u\, du}$$

as a function of depth (z)-normalized GPP and the photon flux density in the photosynthetic range (PPFD, μmol m^{-2} d^{-1}). Areal rate of respiration is given by (Eq. 3):

(3) $R_t = \frac{ER}{z}$

The instantaneous gas exchange rate D_t (g O_2 m^{-3} d^{-1}), is described by Eq. 4:

(4) $D_t = K_{2,t} \times (O\ sat_{t-\Delta t} - O\ mod_{t-\Delta t})$

where $K_{2,t}$ (day^{-1}) is the O_2-specific gas exchange coefficient, O_{sat} is the equilibrium concentration of dissolved oxygen at saturation, and O_{mod} is the modeled oxygen concentration. The model fits a daily value of K_{600}, the gas exchange coefficient for oxygen normalized to a Schmidt number of 600, reflecting oxygen concentraion at 17.5 °C.

To avoid equifinality in parameter estimates, we used a Bayesian state-space statistical approach, separately estimating process and observation errors. Differences between observed and modeled oxygen concentrations are attributed to observation error as Eq. 5:

(5) $O_{obs,t} = O_{mod,t} + \varepsilon_{obs,t}$

where $O_{obs,t}$ is the observed concentration of dissolved oxygen at time, t, $O_{mod,t}$ is the corresponding modeled concentration and $\varepsilon_{obs,t}$ is observation error. Modeled oxygen at time *t* is a function of the change in oxygen concentration between timesteps and process error (Eq. 6):

(6) $O_{mod,t} = O_{mod,t-\Delta t} + \int_{u=t-\Delta t}^{t} (\frac{dO_{mod,u}}{du} + \varepsilon_{proc,u}) du$

where $\varepsilon_{proc,u}$ is process error at time, *u*.

We used a partial pooling approach to estimate K_{600}, relating daily values of K_{600} to discharge (Q). The gas-evasion rate is determined by turbulence at the air-water interface, which is related to river discharge (Raymond et al. 2012). Partial pooling is effective by attributing error in K to processes in addition to variation in Q. We allowed each daily estimate of K_{600} to deviate from the pooling prediction by an error term with standard deviation σ_{K600}.

We applied the default, normally-distributed priors recommended by Appling et al. (2018), as derived from estimates of metabolism compiled by Hall et al. (2016), with modifications as described as follows:

(7) $GPP \sim \mathcal{N}(3.1, 6.0)$

(8) $ER \sim \mathcal{N}(-7.1, 7.1)$

(9) $K_{600} \sim \mathcal{N}(K_{600,pred}(Q_d), \sigma_{K600})$

where σ_{K600} describes deviation of K_{600} from the pooling prediction and the distributions for GPP and ER were truncated at zero. We report rates of GPP and ER following the convention of positive values for production and negative values for respiration.

We ran the model separately for each of the two years. For each model run, we used four MCMC chains run on four cores in parallel for 9,000 warmup steps and 1,500 saved steps. Models were fit in R (version: 4.2.2) using Stan (*rstan* version 2.26.13), and *StreamMetabolizer* (version 0.12.0). We visually inspected trace plots of MCMC samples for mixing and assessed convergence of parameter estimates with the $\hat{R}$ metric, which compares within- and between-chain variance, and applied an upper threshold of 1.01 to establish convergence.

Results

Water quality

Water chemistry followed patterns typical of upland streams and rivers in Interior Alaska (Tables 2 & 3). Lower concentrations of inorganic solutes during snowmelt transitioned to increasingly elevated concentrations, especially of calcium, magnesium, sulfate, and nitrate, following spring freshet (Figs. 3 & 4). Dissolved organic carbon and TDP showed opposite patterns to inorganic constituents, with elevated concentrations during snowmelt rapidly declining with recession to baseflow (Figs. 3 & 4). All chemical

constituents were within Alaska water quality standards for recreation, drinking, and/or aquatic life (Tables 3 & 4). However, water temperature exceeded the standards for anadromous salmonids (Tables 2 & 3). Temperatures exceeded thresholds for salmonids for much of mid-June to early August in 2021 and in mid-June to early July of 2022. However, water temperature rarely exceeded 18^{o}C, a threshold associated with heat stress in chinook of the Yukon River Basin (von Biela et al. 2020).

Table 2. Summary of measured constituents in the Salcha River (2021) with comparison to AK water quality standards.

Constituent	**Mean**	**Median**	**Min**	**Max**	**SD**	**Standard**	
	2021					Aquatic Life	Recreation/Drinking Water
fDOM (QSU)	60.85	54.1	38.16	153.17	21.04		
Dissolved oxygen (mg/L)	10.84	10.58	8.89	14.14	1.06	>4 & < 17 mg/L; >7 mg/L for anadromous fish; >5 mg/L for non-anadromous fish	
pH	7.61	7.63	7.23	7.82	0.11	6.5 - 8.5; not vary by 0.5 from natural condition	6.5 - 8.5
Specific conductivity (µS cm^{-1})	209.8	220.3	126.6	251.8	28.4		
Temperature (°C)	10.7	10.44	-0.01	18.46	4.23	<20°C; Migration routes < 15°C Spawning areas < 13°C Rearing areas < 15°C Egg /fry incubation < 13°C	<15°C
Turbidity (FNU)	2.03	1.57	0.01	17.74	1.61	<25 NTU above natural conditions	<5 NTU above natural condition when NTU is below 50
Ammonium (µM)	0.5	0.1	0.1	1.5	0.6		
Bromide (µM)	0.1	0.1	0.1	0.1	0		
Calcium (µM)	679.9	723.9	443.1	805.4	116.3		
Chloride (µM)	8.9	7.1	5.5	24.8	5.1	6488 (chronic)	
Fluoride (µM)	6.3	5.9	4.2	11.9	1.9		210.5
Magnesium (µM)	293.7	315.5	202	349.1	47.6		
Nitrate (µM)	20.6	21.1	16	26.6	3.7		714
Dissolved organic carbon (µM)	333	250	199	783	169		
Potassium (µM)	23.9	24.5	20.4	27.2	2.2		
Sodium (µM)	94.5	102.2	61	110.6	17.3		
Sulfate (µM)	495.6	506.8	235.5	744.2	142.2		2839
Total dissolved phosphorus (µM)	0.1	0.1	0.1	0.2	0		
Total dissolved nitrogen (µM)	28.5	27.3	20.2	39.5	6.2		

Table 3. Summary of measured constituents in the Salcha River (2022) with comparison to AK water quality standards.

Constituent	Mean	Median	Min	Max	SD	Standard	
	2022					Aquatic Life	Recreation/Drinking Water
fDOM (QSU)	87.74	60.51	44.21	295.75	59.36		
Dissolved oxygen (mg/L)	11.1	10.84	9.23	13.25	0.92	>4 & < 17 mg/L; >7 mg/L for anadromous fish; >5 mg/L for non-anadromous fish	
pH	7.49	7.57	6.9	7.85	0.22	6.5 - 8.5; not vary by 0.5 from natural condition	6.5 - 8.5
Specific conductivity (µS cm^{-1})	191.9	216.9	75.6	245.1	53.0		
Temperature (ºC)	8.71	9.81	0	16.78	3.93	<20°C; Migration routes < 15°C Spawning areas < 13°C Rearing areas < 15°C Egg /fry incubation < 13°C	<15°C
Turbidity (FNU)	5.07	1.37	0.03	76.82	8.36	<25 NTU above natural conditions	<5 NTU above natural condition when NTU is below 50
Ammonium (µM)	0.2	0.1	0.1	0.5	0.1		
Bromide (uM)	0.1	0.1	0.1	0.2	0		
Calcium (µM)	697.1	804.9	329.2	878.4	198		
Chloride (µM)	7.9	7.1	6	12.2	2.2	6488 (chronic)	
Fluoride (µM)	4.1	3.9	2.7	7.5	1.3		210.5
Magnesium (µM)	312.8	349.8	170.4	402.7	83.3		
Nitrate (µM)	19.9	17.1	8.5	31.8	7.7		714
Dissolved organic carbon (µM)	600	310	254	2154	608		
Potassium (µM)	27.5	28.1	22.7	30.2	2.5		
Sodium (µM)	94.1	104.8	58.6	110.7	19.3		
Sulfate (µM)	553.3	525.1	190.9	945.6	226.7		2839
Total dissolved phosphorus (µM)	0.1	0.1	0.025	0.4	0.1		
Total dissolved nitrogen (µM)	40.9	34.4	28.8	90.1	18.4		

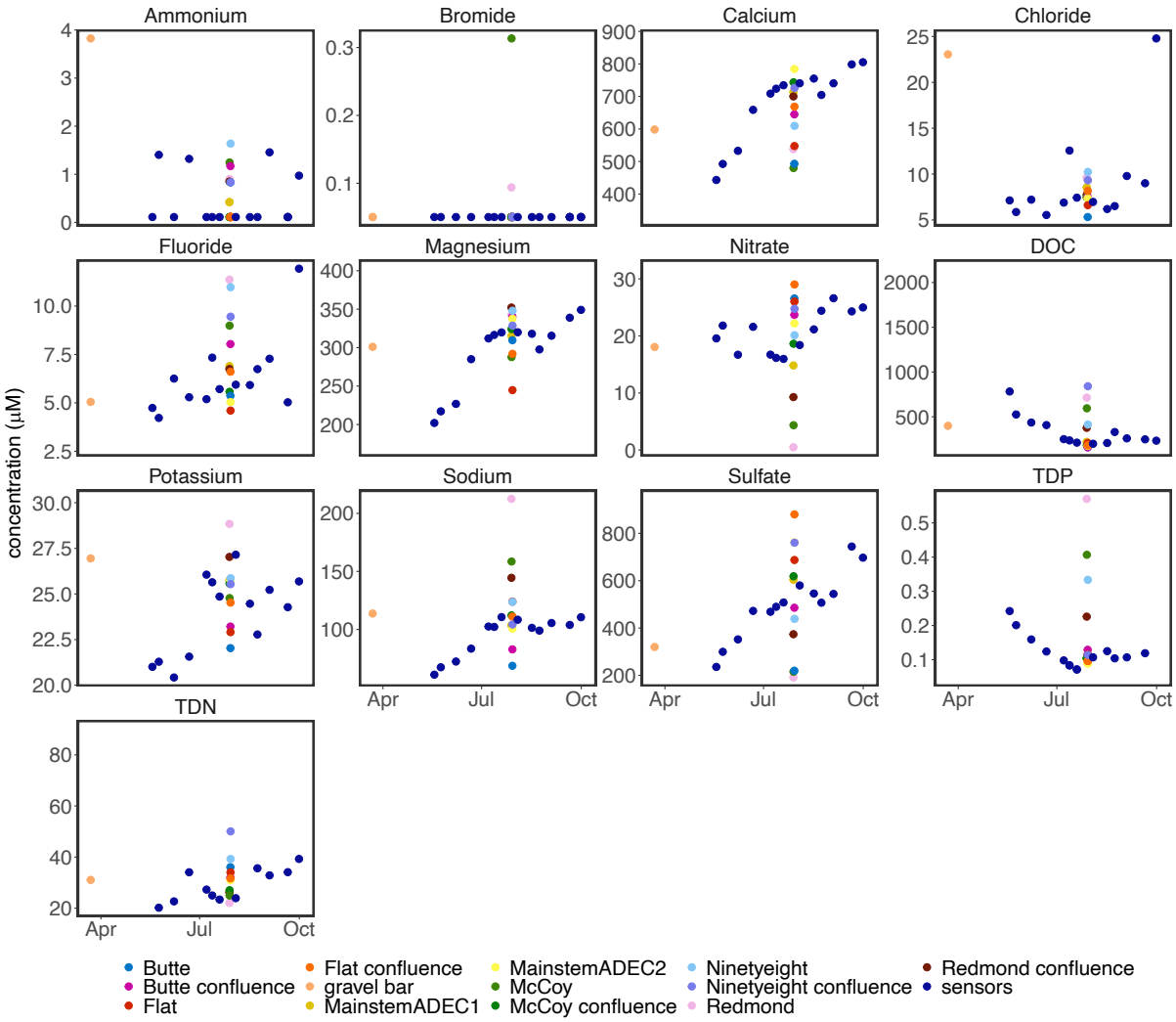

Figure 3. Solute concentrations measured in the Salcha River, selected tributaries, and corresponding confluences in 2021. Biweekly samples from the mainstem were collected at the location of sensor deployment near the USGS gauging station.

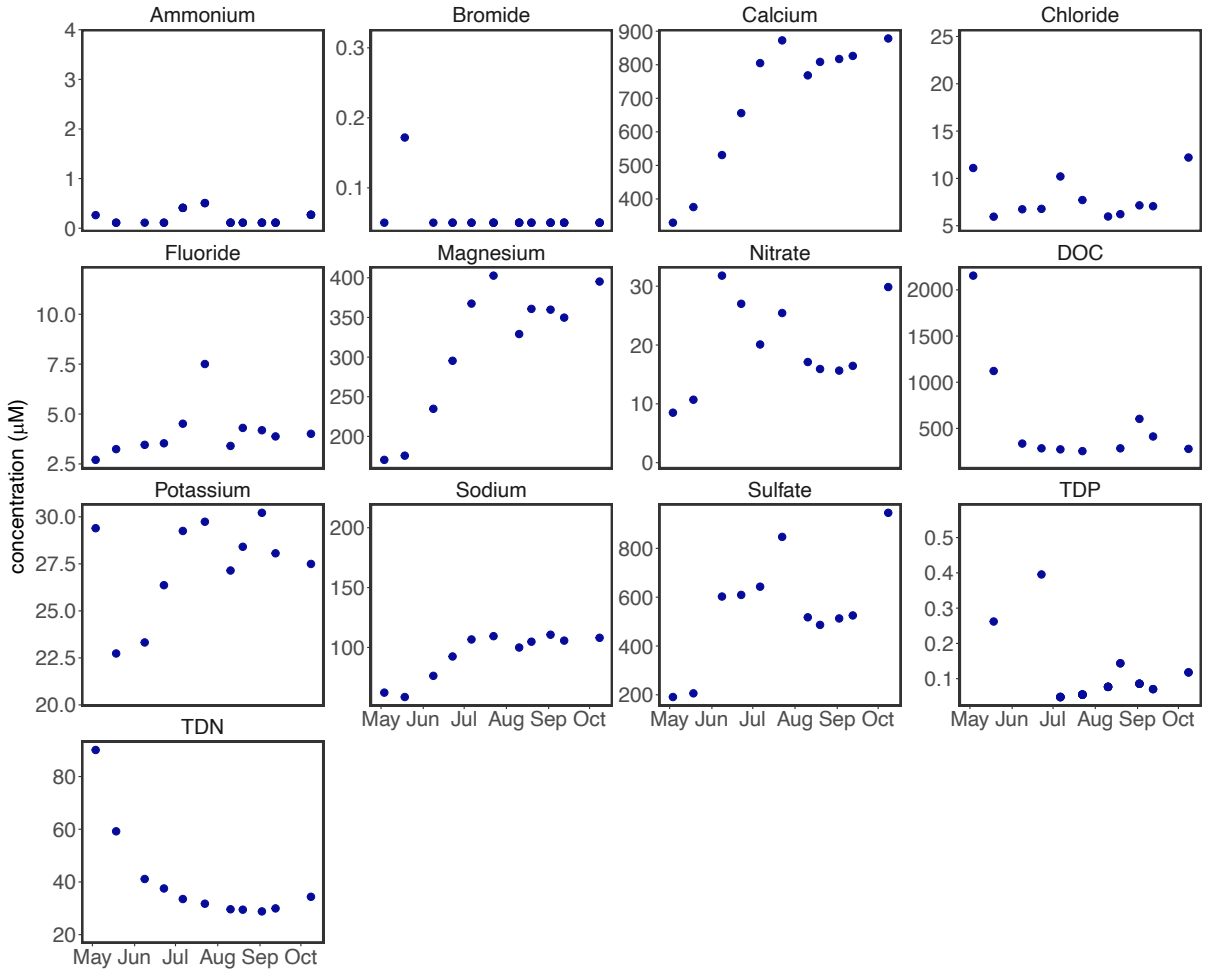

Figure 4. Solute concentrations measured in the Salcha River in 2022. Biweekly samples from the mainstem were collected at the location of sensor deployment near the USGS gauging station.

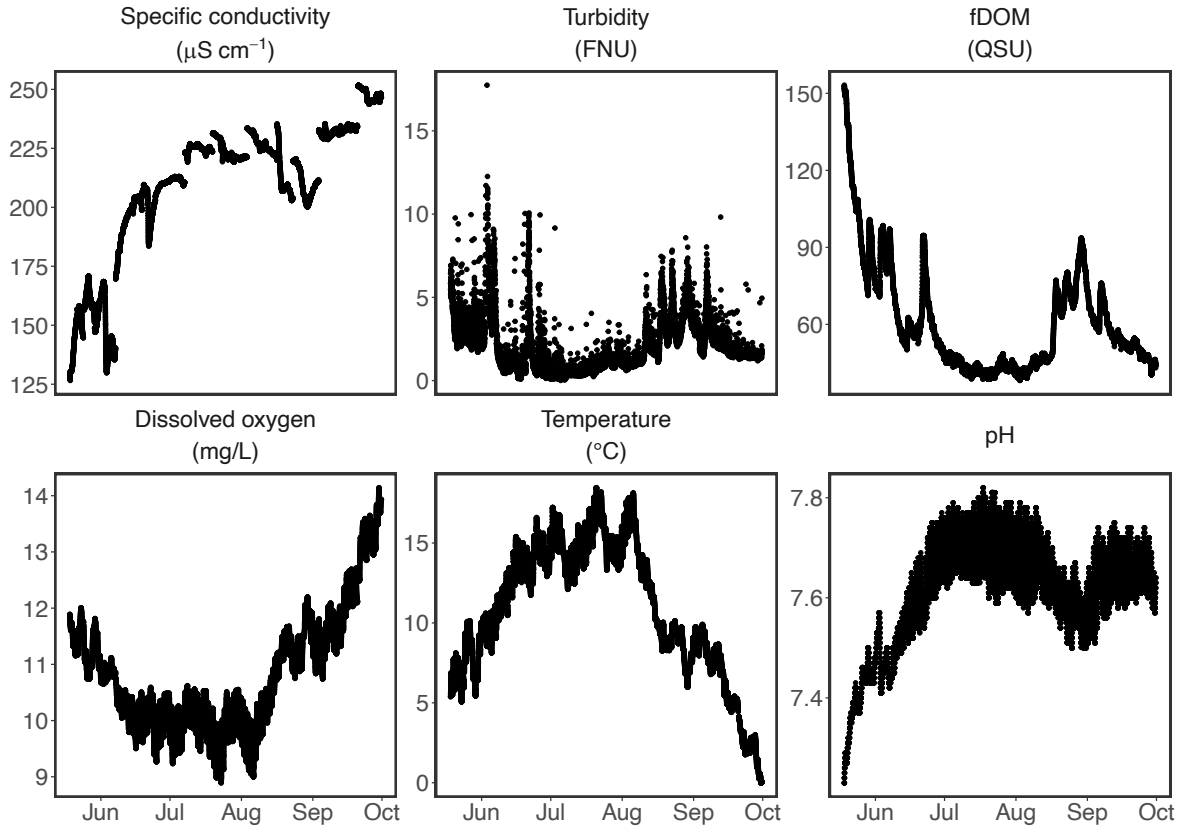

Figure 5. Stream temperature and chemistry monitored at 15-min intervals on the mainstem Salcha River in 2021.

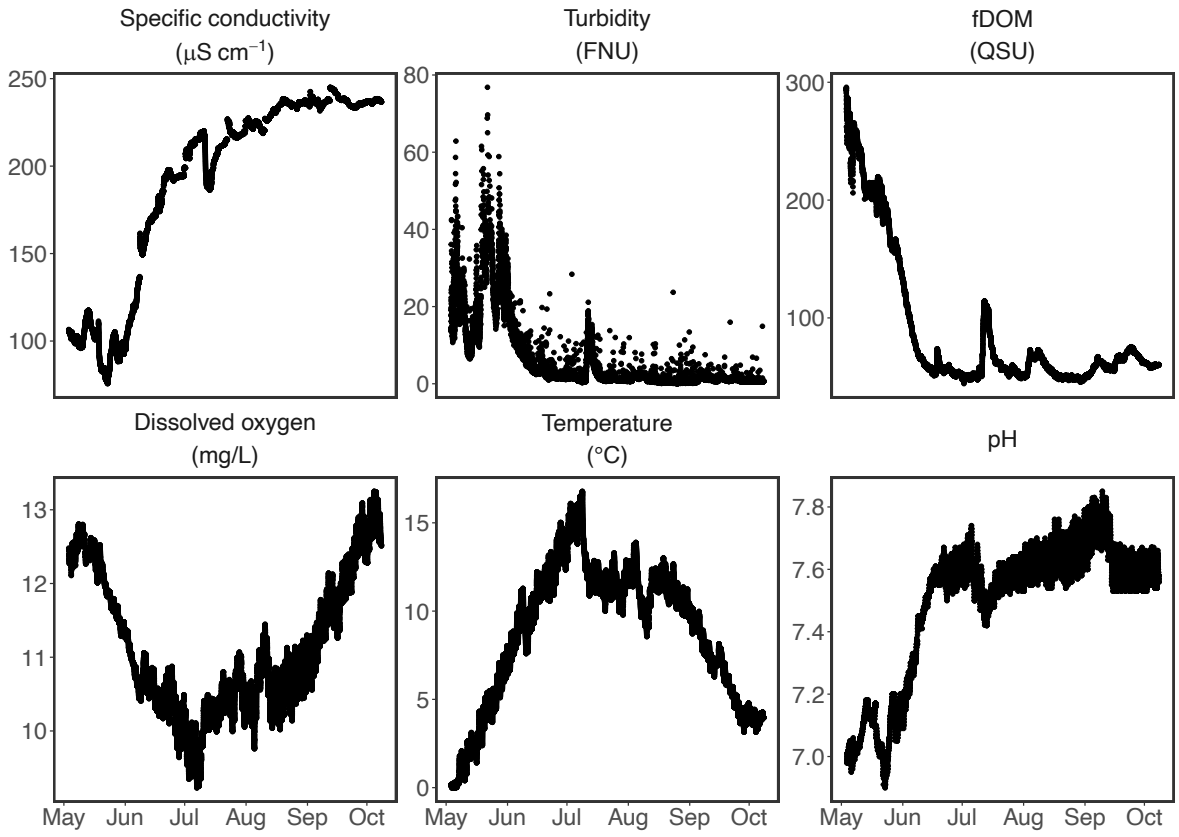

Figure 6. Stream temperature and chemistry monitored at 15-min intervals on the mainstem Salcha River in 2022.

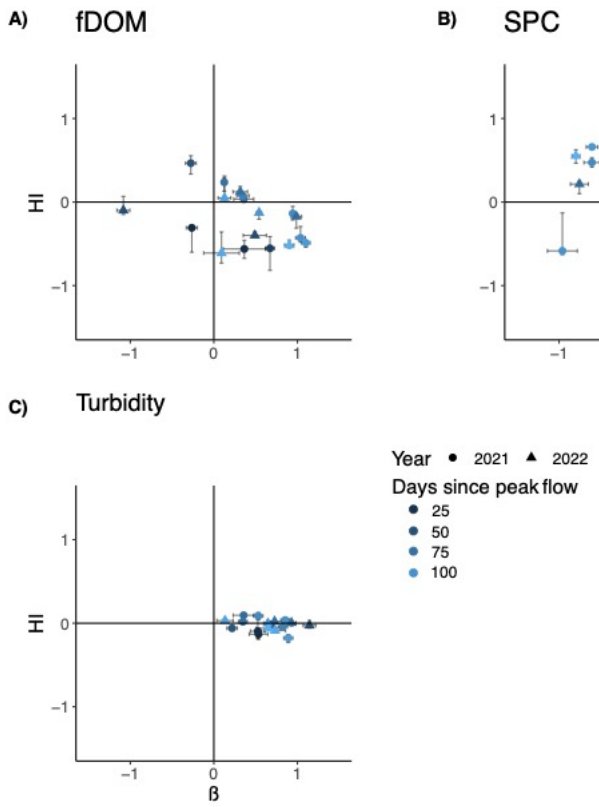

Figure 7. Concentration-discharge relationships during storms for A) fDOM, B) specific conductivity, and C) Turbidity. Positive hysteresis index (HI) indicates clockwise hysteresis in the C-Q relationship (greater concentration relative to discharge on the rising limb of the storm) and negative values indicate counterclockwise hysteresis. Positive values of β indicate flushing of the solute during the storm and negative values indicate dilution.

Storm concentration-discharge dynamics

We identified 19 storms during the study period (open water period of 2021-2022). Fluorescent DOM was typically flushed (+β) from the catchment to the river during storms (Fig. 7A). The C-Q relationship for fDOM indicated significant hysteresis, but the direction varied across storms, as discussed in detail below (Fig. 7A). Specific conductivity was diluted on the rising limb of most storms (-β) and hysteresis was most often clockwise (+HI) indicating either mobilization of nearstream sources of ions contributing to conductivity, or that event water diluted the more concentrated groundwater supplying baseflow (Fig. 7B). Turbidity increased significantly on the rising limb of all storms (+β), though the C-Q relationship was rarey hysteretic (Fig. 7C), likely indicating near- or within-channel mobilization of sediments during storms.

Cumulative precipitation varied several-fold at extents from one week to three months during the period of monitoring and increased linearly with time since peak discharge during spring freshet (Table 4). Likewise, mean temperature during storms declined throughout the monitoring period and weekly mean temperature preceding each storm peaked ~60 days following peak snowmelt discharge (~mid-Jul). Given these correlations among candidate predictors of storm C-Q dynamics and the limited number of events (n=19 storms), multiple regression models explaining variation in storm C-Q dynamics were limited to two uncorrelated predictors: days since peak flow and weekly mean temperature.

A linear model explained 28% of the variation in HI-fDOM, where HI-fDOM = -0.172 + 0.198*temperature + 0.108*days since peak flow, with coefficients representing standardized effect sizes and a significant effect of temperature. However, likely due to interactive effects between seasonality of primary production, thaw depth, and

Table 4. Moisture and temperature conditions preceding and during storms (n=19) during the open water period of 2021-2022.

Attribute	Mean	Min	Max
Storm size (mm)	16.2	0.1	76.4
One-week cumulative precipitation (mm)	20.2	0.1	79.1
One-month cumulative precipitation (mm)	52.9	1.5	153.7
Three-month cumulative precipitation (mm)	101.8	1.5	235.3
Mean temperature during storm (°C)	8.6	7.6	17.7
Weekly mean temperature (°C)	11.1	–4.4	18.9

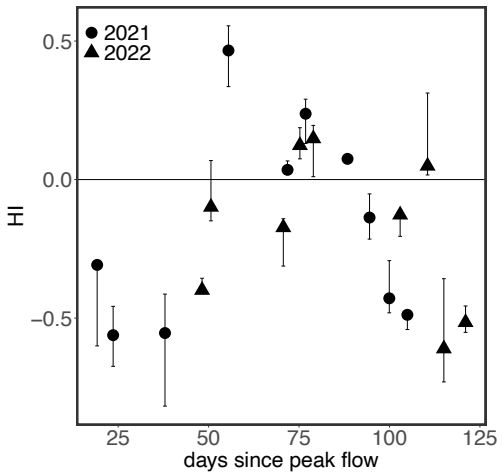

Figure 8. Relationship between the hysteresis index (HI) for fDOM and time since peak snowmelt runoff.

temperature, a non-linear relationship emerged between hysteresis in the C-Q relationship for fDOM during storms and time since peak flow (Fig. 8). Clockwise (source-limited) hysteresis occurred during the mid-summer period of peak temperature and high terrestrial productivity, whereas counterclockwise hysteresis occurred during storms under cooler conditions earlier and later in the season. Riparian or instream primary producers might have been sources of fDOM to the river during the summertime peak in primary productivity, generating this pattern. The same regression model explained less than 20% of the observed variation in the β metric among storms, likely due to non-linear relationships.

HI-turbidity was significantly and positively related to both weekly mean temperature and days since peak flow: HI-turbidity = -0.022 + 0.046*weekly mean temperature + 0.037*days since peak flow, with significant effects of both predictors and R^2=0.34. These positive relationships suggest more rapid mobilization of sediment as cumulative precipitation increased, likely establishing hydrologic connectivity between the river and sediment pools susceptible to export. However, the same model explained less than 10% of the variation in β for turbidity. Finally, storm C-Q relationships for specific conductivity were not significantly related to temperature or seasonality, and regression models explained less than 20% of the observed variation in C-Q relationships.

Sources of water and solutes

An end-member mixing model described seasonal patterns in the sources of water and solutes to the mainstem Salcha River near its confluence with the Tanana River (Fig. 9). On average, across both years of monitoring, we estimated that Ninetyeight Creek contributed 58.3 ± 8.4% of water and solutes to the mainstem, Butte Creek contributed 21.7 ± 5.7%, precipitation contributed 13.5% ± 3.3%, Flat Creek contributed 4.9 ± 5.1%, McCoy Creek contributed 0.9 ± 0.8 %, and Redmond Creek contributed 0.7 ± 0.6%. Though the largest tributaries by contributing area, the north-facing Redmond, McCoy, and Flat creeks did not contribute more than 12% each on any day sampled. Precipitation had the largest average contribution before June, transitioning to dominant inputs of waters reflecting the chemistry of Ninetyeight Creek as snowmelt receded to baseflow and thereafter. Thus, water and solutes are

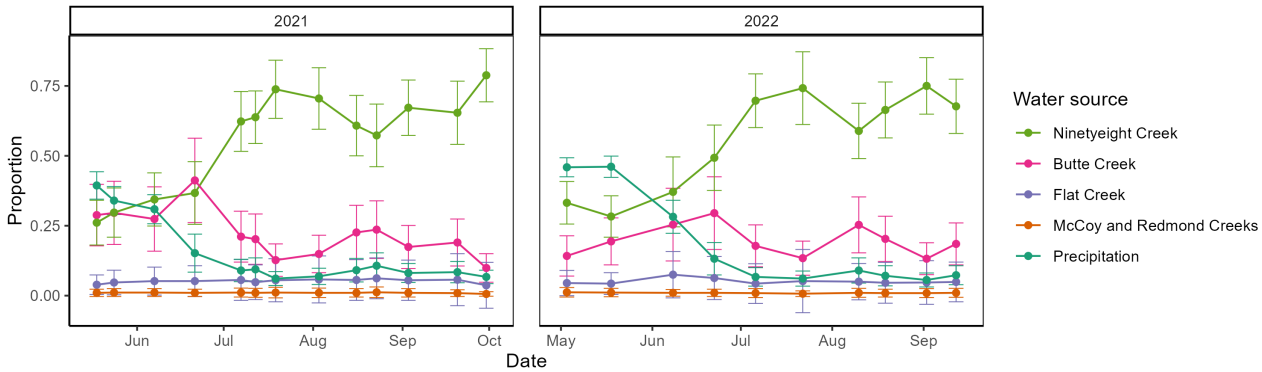

Figure 9. Sources of water and solutes to the mainstem Salcha River at the USGS gauging station. Proportional estimates were derived from an end-member mixing model based on conservative solutes in major tributaries and precipitation. Error bars indicate 95% credible intervals.

predominantly derived from sources similar to the south-facing tributaries, despite the smaller contributing areas of these catchments relative to the sampled north-facing tributaries (Fig. 2, Table 2).

In-stream metabolism

The Salcha River was net heterotrophic (GPP/ER < 1) during both study years. Estimated gross primary production was strongly seasonal (Fig. 10). Gross primary production was negligible during ice-out and peak flow conditions during freshet, then increased to a maximum of ~2.25 g O_2 m^{-2} d^{-1} in late June. This rate is similar to the median of peak summertime rates in streams and rivers of the contiguous US receiving high light input and stable discharge (Bernhardt et al. 2022) and at least three times greater than rates measured in Arctic rivers of Alaska (Rocher-Ros et al. 2021). The maximum rate of productivity in the Salcha was sustained until it declined at the onset of summer rain. Though GPP increased again following large storms, it never returned to the pre-storm maximum. In both years, GPP began to decline in early August, and reached a minimum of about 0.5 g O_2 m^{-2} d^{-1} by the end of monitoring in late Sept/early Oct.

Rates of ER were less temporally dynamic, reaching a maximum of ~–5 g O_2 m^{-2} d^{-1} during the spring freshet of 2021 and ~–7.5 g O_2 m^{-2} d^{-1} during the same period of 2022. Ecosystem respiration then declined to ~–2.5 g O_2 m^{-2} d^{-1} following snowmelt recession and remained relatively constant for the remainder of the monitoring period with the exception of brief increases during a large storm in 2022. Summertime rates of ER were slightly greater than observed in streams of the contiguous US (Bernhardt et al. 2022) and comparable to rates in Arctic streams of Alaska (Rocher-Ros et al. 2021). However, caution must be applied in interpreting modeled rates of ER during 2022, when estimates of ER were strongly correlated with estimates of gas evasion (K, r^2 = –0.48; Fig. A1).

In addition to influence on water quality and carbon flux, metabolic rates are important to salmon productivity, as chinook salmon exhibit density dependence in the Salcha River (Cunningham et al. 2018,

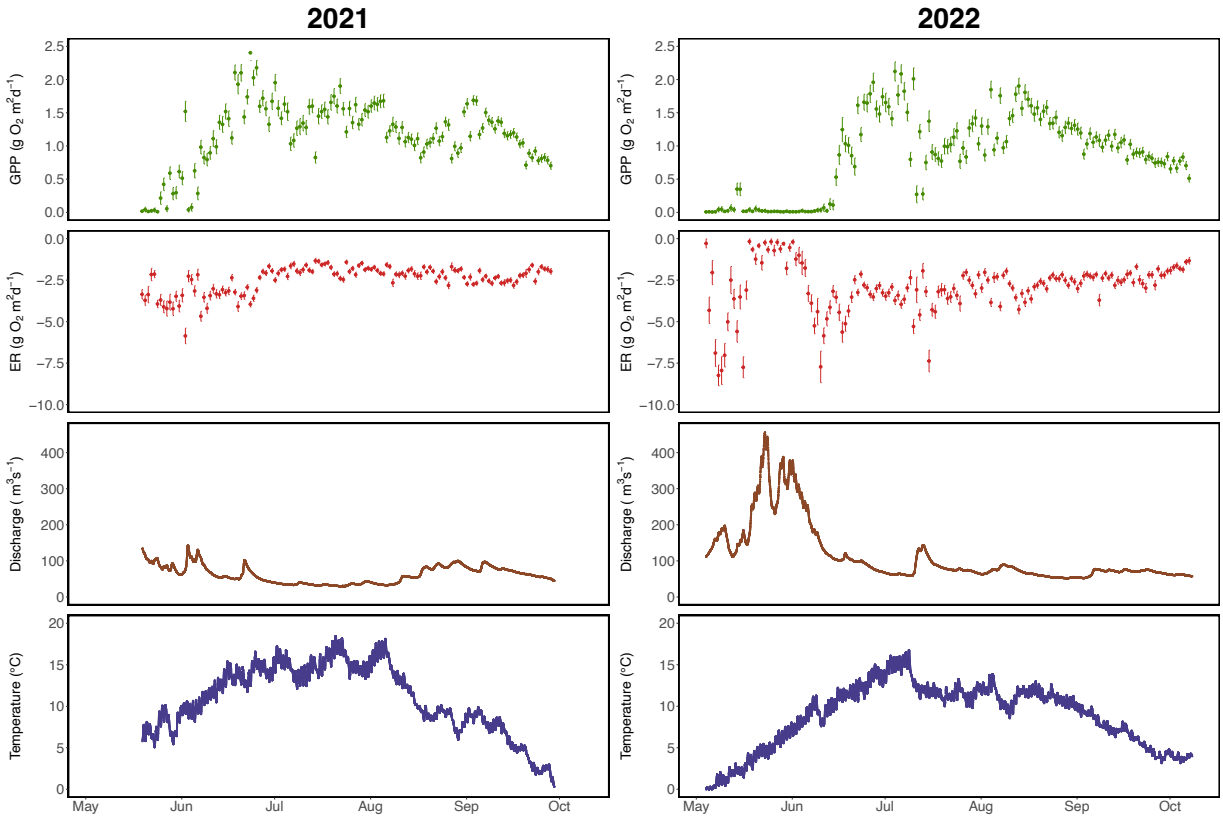

Figure. 10. Estimated rates of gross primary production (GPP) and ecosystem respiration (ER) with discharge and water temperature in the Salcha River.

Neuswanger et al. 2015). Temporal patterns of GPP indicate that stormflows diminish productivity, which could reduce salmon recruitment during years with more storms.

Conclusion

High-frequency observations combined with biweekly grab sampling established minimal influence of the water quality of the Salcha River during the open water period. Concentrations of all measured chemical constituents were below thresholds established for water quality of Alaskan waters used for drinking, recreation, and by aquatic life. Water temperature exceeded thresholds established for salmonids during summer of both 2021 and 2022. Observations emphasize temporal variation in chemistry and instream productivity influenced by stream discharge and seasonality. Flushing of organic solutes during snowmelt and during storms emphasized connectivity of shallow flowpaths to the river early in the thaw season and following precipitation. Inorganic solutes, likely derived from deeper groundwater, showed opposing patterns, and increased later in the season. Regular monitoring referenced to these conditions could track potential changes to the Salcha catchment and its water quality resulting from continued changes in temperature, precipitation, or fire regimes and land development in the watershed.

Literature cited

Appling, A. P., R. O. Hall, C. B. Yackulic, and M. Arroita. 2018. Overcoming Equifinality: Leveraging Long Time Series for Stream Metabolism Estimation. *Journal of Geophysical Research: Biogeosciences* 123:624–645.

Bencala, K. E., McKnight, D. M., & Zellweger, G. W. 1987. Evaluation of natural tracers in an acidic and metal-rich stream. *Water Resources Research* 23(5), 827-836.

Bernhardt, E. S., P. Savoy, M. J. Vlah, A. P. Appling, L. E. Koenig, R. O. Hall, M. Arroita, J. R. Blaszczak, A. M. Carter, M. Cohen, J. W. Harvey, J. B. Heffernan, A. M. Helton, J. D. Hosen, L. Kirk, W. H. McDowell, E. H. Stanley, C. B. Yackulic, and N. B. Grimm. 2022. Light and flow regimes regulate the metabolism of rivers. *Proceedings of the National Academy of Sciences* 119:e2121976119.

Cunningham, C. J., P. A. H. Westley, and M. D. Adkison. 2018. Signals of large scale climate drivers, hatchery enhancement, and marine factors in Yukon River Chinook salmon survival revealed with a Bayesian life history model. *Global Change Biology* 24:4399–4416.

De Filippi, F. M., Iacurto, S., Grelle, G., & Sappa, G. 2021. Magnesium as environmental tracer for karst spring baseflow/overflow assessment—A case study of the Pertuso Karst Spring (Latium Region, Italy). *Water* 13(1), 93.

Godsey, S. E., J. W. Kirchner, and D. W. Clow. 2009. Concentration-discharge relationships reflect chemostatic characteristics of US catchments. *Hydrological Processes* 23:1844–1864.

Hall, R. O., J. L. Tank, M. A. Baker, E. J. Rosi-Marshall, and E. R. Hotchkiss. 2016. Metabolism, gas exchange, and carbon spiraling in rivers. *Ecosystems* 19:73–86.

Lloyd, C. E. M., J. E. Freer, P. J. Johnes, and A. L. Collins. 2016. Using hysteresis analysis of high-resolution water quality monitoring data, including uncertainty, to infer controls on nutrient and sediment transfer in catchments. *Science of the Total Environment* 543:388–404.

Neuswanger, J. R., M. S. Wipfli, M. J. Evenson, N. F. Hughes, and A. E. Rosenberger. 2015. Low productivity of Chinook salmon strongly correlates with high summer stream discharge in two Alaskan rivers in the Yukon drainage. Canadian Journal of Fisheries and Aquatic Sciences 72:1125–1137.

Odum, H. T. 1956. Primary production in flowing waters. *Limnology and Oceanography* 1:102–117.

Raymond, P. A., C. J. Zappa, D. Butman, T. L. Bott, J. Potter, P. Mulholland, A. E. Laursen, W. H. McDowell, and D. Newbold. 2012. Scaling the gas transfer velocity and hydraulic geometry in streams and small rivers: Gas transfer velocity and hydraulic geometry. *Limnology and Oceanography: Fluids and Environments* 2:41–53.

Rocher-Ros, G., T. K. Harms, R. A. Sponseller, M. Väisänen, C. Mörth, and R. Giesler. 2021. Metabolism overrides photo-oxidation in CO_2 dynamics of Arctic permafrost streams. *Limnology and Oceanography* 66: S169-181.

Schemel, L.E.; Cox, M.H.; Runkel, R.L.; Kimball, B.A. Multiple injected and natural conservative tracers quantify mixing in a stream confluence affected by acid mine drainage near Silverton, Colorado. *Hydrological Processes* 2006, 20, 2727–2743.

Stock, B. C., Jackson, A. L., Ward, E. J., Parnell, A. C., Phillips, D. L., & Semmens, B. X. 2018. Analyzing mixing systems using a new generation of Bayesian tracer mixing models. *PeerJ* 6, e5096.

von Biela, V. R., L. Bowen, S. D. McCormick, M. P. Carey, D. S. Donnelly, S. Waters, A. M. Regish, S. M. Laske, R. J. Brown, S. Larson, S. Zuray, and C. E. Zimmerman. 2020. Evidence of prevalent heat stress in Yukon River Chinook salmon. *Canadian Journal of Fisheries and Aquatic Sciences* 77:1878–1892.

Webster, A. J., T. A. Douglas, P. Regier, M. D. Scheuerell, and T. K. Harms. 2021. Multi-scale temporal patterns in stream biogeochemistry indicate linked permafrost and ecological dynamics of boreal catchments. *Ecosystems* 25: 1189-1206.

Appendix 1

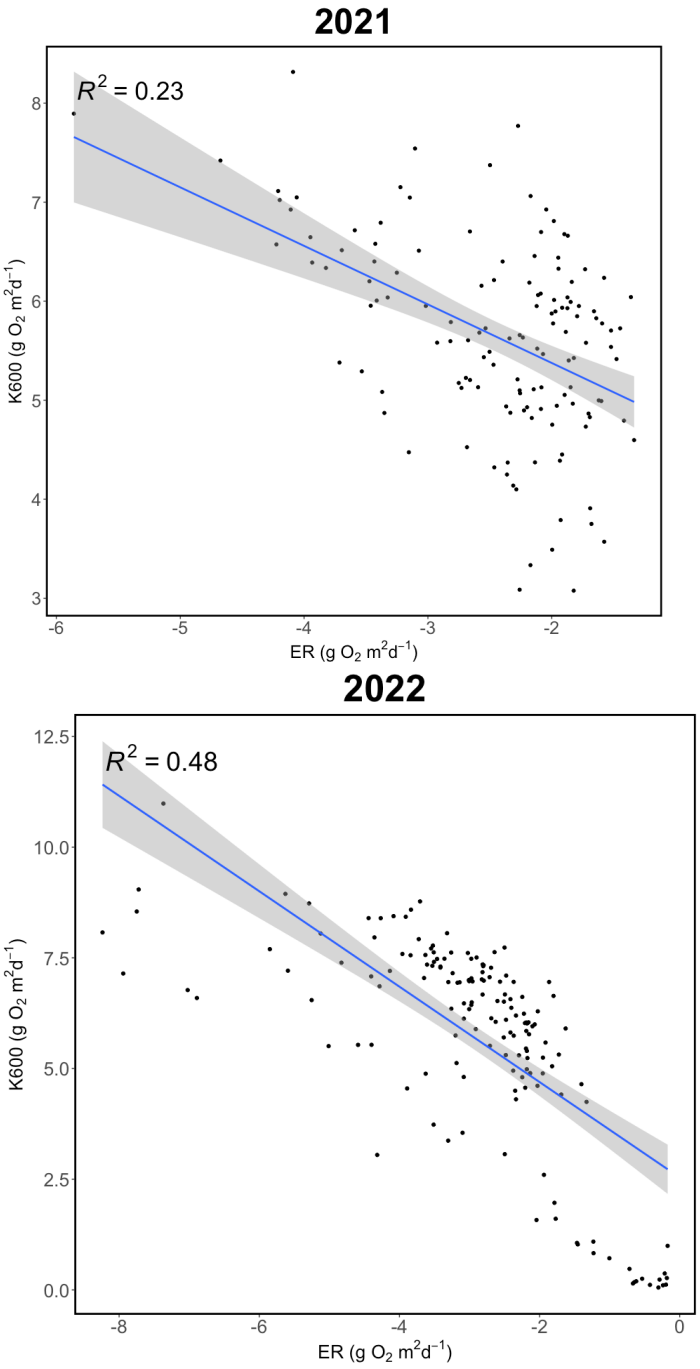

Figure A1. Correlation of modeled rates of ecosystem respiration (ER) and gas evasion (K600).